A Novel Tractable Methodology to Stochastic Multi-Period AC OPF in Active Distribution Systems Using Sequential Linearization Algorithm

Muhammad Usman , *Member, IEEE*, and Florin Capitanescu , *Member, IEEE*

Abstract—The ongoing transition of passive distribution networks to active distribution systems (ADSs) calls for the development of sophisticated and tractable tools to address the needs and challenges of future ADSs. In this regard, this work proposes a novel tractable methodology for flexibility procurement via stochastic multi-period AC optimal power flow (S-MP-OPF). The first novelty of the proposed methodology is the formulation of a new mixed-integer linear programming (MILP) model, which develops novel linear approximations for all nonlinear constraints (i.e., active and reactive power flows and branch currents) that ensure tractability. The proposed linearization approach relies on the second-order Taylor series expansion of trigonometric terms, does not hinge on the flat-voltage, near-voltage and small angle assumptions, and formulates the linear approximations using square of voltage magnitude and voltage angle difference variables. The second novelty is a sophisticated heuristic sequential linearization algorithm (SLA) which incorporates and improves the accuracy of the MILP model in an iterative manner. The bench-marking of proposed SLA is done on a 34-bus ADS for a comprehensive set of flexible options, whereas its versatility and scalability is demonstrated on real-world 31-bus weakly-meshed and 191-bus radial ADSs. Extensive numerical analyses show that the proposed SLA leads to a highly accurate and feasible solution with small optimality gap within few iterations, under normal and stressed operating conditions, outperforms alternative methods in terms of solution accuracy and computational efficiency, and is scalable to large S-MP-OPF problems.

Index Terms—Active distribution systems, flexibility, multi-period optimal power flow, stochastic optimization, tractability.

NOMENCLATURE

Sets

N	set of nodes.
G	set of renewable energy sources (RES).
B	set of electrical energy storages (EES).
F	set of flexible loads (FLs).
E	set of HV/MV substations.
L/L^c	set of lines/set of lines in a cycle.
L^T	set of on-load tap changer (OLTC) transformers.
Y	set of discrete values of OLTC transformer ratio.
T/S	set of time-periods/scenarios.

Optimization Variables (in period t and scenario s)

$P^e_{i,s,t}$	active power flow from HV upstream grid at bus i.
$Q^e_{i,s,t}$	reactive power flow from HV upstream grid at bus i.
$P^{curt}_{i,s,t}$	amount of RES curtailed generation at bus i.
$Q^{RES}_{i,s,t}$	reactive power provision from RES at bus i.
$P^{ch}_{i,s,t}$	active power charging of EES at bus i.
$P^{dch}_{i,s,t}$	active power discharging of EES at bus i.
$P^{od}_{i,s,t}$	active power overdemand of FL at bus i.
$P^{ud}_{i,s,t}$	active power underdemand of FL at bus i.
$\beta^{ch}_{i,s,t}$	binary variable representing EES charging at bus i.
$\chi^{od}_{i,s,t}$	binary variable representing FL overdemand at bus i.
$\mu^k_{if,s,t}$	binary variable representing k-th ratio of OLTC if.
$\lambda^k_{if,s,t}$	auxiliary variable representing $\mu^k_{if,s,t} \cdot V^2_{i,s,t}$.
$SoC_{i,s,t}$	State-of-Charge (SoC) of EES at bus i.
$V^2_{i,s,t}$	square of voltage magnitude at bus i.
$\theta_{ij,s,t}$	voltage angle difference between nodes i and j.

Parameters (in period t and scenario s)

g_{ij}	conductance of the branch linking buses i and j.
b_{ij}	susceptance of the branch linking buses i and j.
$P^0_{i,s,t}$	available active power of RES unit at bus i.
$P^d_{i,s,t}/Q^d_{i,s,t}$	active/reactive power demand at bus i.
$\varphi_{i,s,t}$	angle defining load power factor $\cos(\varphi_{i,s,t})$.
$\phi_{i,s,t}$	angle defining RES power factor $\cos(\phi_{i,s,t})$.
$P^{ch,r}_i$	rated active power charging of EES at bus i.
$P^{dch,r}_i$	rated active power discharging of EES at bus i.
E^r_i	rated energy capacity of EES at bus i.
η^{ch}_i/η^{dch}_i	charging/discharging efficiency of EES at bus i.
r^k_{if}	k-th discrete ratio value of OLTC if.
$\underline{x}/\overline{x}$	minimum/maximum value of x (e.g., V, SoC).
ΔT	duration of time period t.
M	demand flexibility factor as % of available load.
$c^{curt}_{i,p}$	cost (€/MWh) of curtailed active power at bus i.
$c^{str}_{i,b}$	cost (€/MWh) of usage of storage at bus i.
$c^{fl}_{i,l}$	cost (€/MWh) of demand flexibility at bus i.

c_{ij}^{oltc} cost (€) of operation of OLTC transformer.

π_s probability of scenario s.

I. INTRODUCTION

A. Motivation

The accelerated integration of distributed energy resources (DER), such as variable renewable energy sources (RES), mainly wind and solar, electrical energy storages (EESs) and flexible loads (FLs), have altered the passive nature of distribution networks, enforcing their transition to active distribution systems (ADSs) [1]. On the one hand, the variable power production from RES brings additional challenges to distribution system operators (DSOs) e.g., voltage rise or congestion [2]; on the other hand, enabling DER controllability leads to the availability of additional flexibility which can be exploited by DSOs to ensure a more reliable and cost-efficient network operation. Under such paradigm, it becomes imperative to manage ADSs in an optimal manner, thus utilizing the full potential of their flexibility. In this regard, advanced scalable network operation methodologies, which address optimally the needs and challenges of future ADSs are need of the hour.

One of the main requirements pertaining to future ADSs is the procurement of flexibility by DSOs, via stochastic multi-period optimal power flow (S-MP-OPF) framework, to satisfy their operation constraints. Such a framework in its full formulation, involving uncertainty from RES and inter-temporal aspects of DER, belongs to the class of mixed-integer non-linear programming (MINLP), which is neither tractable nor scalable and, therefore, cannot be used for practical purposes. *In this context, the core motivation of this work is, therefore, to develop a novel tractable methodology for S-MP-OPF framework for flexibility procurement in ADSs.*

B. Related Works

The consideration of RES and/or emerging DER, in *day-ahead* S-MP-OPF flexibility procurement framework in ADSs has been a topic of substantial research [3], [4], [5], [6], [7], [8], [9], [10], [11], [12], [13], [14], [15], [16], [17], [18], [19] in recent years. However, such a framework belongs to the MINLP class whose computational bottleneck arises from (i) the integral modeling of modern DER (EES, FLs) and conventional assets (OLTC transformers), (ii) the challenging size of problem being determined by the product of three-dimensions: network size, number of uncertainty scenarios and number of time-periods and (iii) the non-convex AC power flow equations. Consequently, to handle the computational complexity of MINLP model, simpler optimization models tackling non-convexity, problem dimension or both have been proposed in the literature quite recently. Note that, complementary to the addressed day-ahead stage, the activation of procured flexibility is usually carried out by some *real-time* OPF algorithm [20], [21], [22]; this is outside the scope of this work.

In [3], [4], [5], [6], [7], the proposed models consider only the stochastic nature of RES and ignore the inter-temporal DER, thus leading to a stochastic single-period (S-SP) optimization framework. On the other hand, in [8], [9], [10], inter-temporal DER are modeled along with RES; however, inherent uncertainty associated with RES is disregarded, resulting in a deterministic multi-period (D-MP) optimization framework. In nutshell, both frameworks set aside one salient *dimension* of future ADSs and solve a reduced dimension optimization model, which is incapable of *fully* representing the future ADSs.

To overcome the shortcomings of [3], [4], [5], [6], [7], [8], [9], [10], [11], [12], [13], [14], [15], [16], [17], [18], [19] consider both inter-temporal and probabilistic aspects of DER and RES, respectively. However, either an intractable MINLP model is tackled [12], [13], or tractability is achieved using convex relaxation [14], [15] or approximation techniques [16], [17], [18], [19], under a reduced set of flexibility options.

In [14], [15], the non-convexity of AC power flow equations is handled by second-order cone programming relaxation. However, no guarantee about the feasibility of recovered solution is provided. In [16], [18], linear relation between the voltages and injected powers, originally proposed in [23], is utilized; however, losses terms are ignored in [23]. In [17], binary variables-based piece-wise linear terms are derived to replace the trigonometric function, which inadvertently increases the integral dimension of model under a stochastic multi-period (S-MP) framework. Moreover, the utilization of small voltage variation assumption in [17] does not strictly hold under stressed operating conditions. Lastly, in [19], a linear energy balance equation is formulated but it ignores completely the non-linear power flow equations.

From flexible options point-of-view, only a subset of flexible resources of future ADSs are modeled in [11], [12], [13], [14], [15], [16], [17], [18], [19], mainly focusing on using RES and EES. Accordingly, other flexible assets such as FLs, reactive power provision from RES [11], [12], [13], [14], [15], [16], [17], [18] and OLTC transformer [11], [13], [16], [17], [18], [19] are ignored. Moreover, in the majority of works, EES and FLs are modeled using an approximation of their intrinsic integer model by simply dropping the binary variables [8], [9], [10], [11], [12], [16].

The works in [3], [4], [5], [6], [7], [8], [9], [10], [11], [12], [13], [14], [15], [16], [17], [18], [19] rely on the *model-based* framework which assumes that ADS model is known and trust to sufficient accuracy. Recently, a *model-free (or data-driven)* framework has emerged [24], [25], which employs various machine learning algorithms [26] to quickly approximate an OPF solution. However, there is no mathematical guarantee on the quality of the estimated solution as compared to the model-based OPF framework, which ensures at least a local optimum solution, while in practice often providing the global optimum. Furthermore, although this framework claims to be model-free, it relies on solving a huge number of model-based OPF problems [27] or power flows. Accordingly, the major issues with such algorithms are: dependence on data quality, huge amount of time and memory to build up the training set, unsatisfactory performance under sudden change in operating conditions, etc. To conclude, this framework is still in its infancy and not yet competitive with the model-based framework of this paper.

Finally, the uncertainty modeling of DER in OPF framework are carried out by: stochastic [6], [7], [11], [13], [17], [18], [19], chance constrained [3], [16] or robust [4], [5], [12], [14] optimization techniques. Each of these approaches exhibits well known pros and cons; readers can refer to the above-mentioned works in each category for better understanding. This paper opts for stochastic optimization as the proposed algorithm can be fed with a reasonable number of scenarios without compromising its computation time.

C. Paper Contributions

From the literature review, one can conclude that the existing methodologies do not consider all flexible options that can be envisioned in future ADSs as well as rely on convex relaxation or single-step linearization approaches to foster tractability. However, convex relaxations provide AC feasible solution only under stringent conditions [28], which are usually impractical to achieve in real-world power systems. Similarly, the explored linearization techniques are single step, largely based on small voltage deviation assumption around the linearization point, fail to model the impact of losses and therefore lead to inaccurate solution under stringent network operating conditions. To overcome the shortcomings of existing works, a novel tractable methodology, based on the linear approximations of AC power flows and sequential linearization algorithm, is proposed which provides a highly accurate, near-optimal solution as well as retains tractability.

The main contributions of this work are as follows:
1) A novel second-order linear approximation of AC active and reactive power flows, and branch current expression which is based on the *square of voltage magnitude* and *voltage angle difference* variables and employs second-order Taylor series expansion of trigonometric terms. Moreover, it linearizes bi-linear voltage magnitude term through a newly introduced term and does not rely on small angle and near/flat voltage profile assumptions as in [29], [30], [31], [32]. Accordingly, it captures more non-linearity than the existing approaches through additional terms (product of voltages magnitude and angle) and implicitly models network losses and their dependency on both voltage magnitude and angle.
2) Based on the proposed linear expressions, a *tractable* mixed-integer linear programming (MILP) model is developed, which considers, unlike existing works, a detailed set of flexible options pertaining to future ADSs.
3) A sequential linearization algorithm (SLA) is proposed under a S-MP-OPF flexibility procurement framework in day-ahead operation planning of ADSs. It incorporates and enhances the accuracy of developed MILP model to improve its accuracy in an iterative manner, and is tested on real-world weakly meshed and radial ADSs to illustrate its versatility and scalability.

Note that linear approximations of active and reactive power flow expressions proposed in [29] are also based on the same decision variable space as ours. However, the resultant expressions capture less non-linearity as compared to the expressions presented in this work, as detailed in Section IV.

TABLE I
KEY FEATURES OF EXISTING APPROACHES

Ref.	Char.	Flexibility Resources		Model Formulation		
		Continuous	Discrete	Accurate	Approx.	Relaxation
[3], [5]	S-SP	RES	OLTC			MISOCP
[4]	S-SP	RES				MISOCP
[6]	S-SP	RES				SOCP
[7]	S-SP	RES	FLs	MINLP		
[8]	D-MP	RES, FLs, EES, ADPF	OLTC		MILP	
[9]	D-MP	EES, FLs		NLP		
[10]	D-MP	RES, EES		NLP		
[11]	S-MP	RES, EES		NLP		
[12]	S-MP	RES, EES	OLTC	MINLP		
[13]	S-MP	RES	EES	MINLP		
[14]	S-MP	RES	EES, OLTC			MISOCP
[15]	S-MP	RES, FLs	EES, OLTC			MISOCP
[16]	S-MP	RES, EES			LP	
[17]	S-MP	RES			MILP	
[18]	S-MP	RES	EES		MILP	
[19]	S-MP	RES	EES, FLs		MILP	
This Work	S-MP	RES, APF	EES, FLs, OLTC		MILP	

Char.: characteristics, Approx.: approximation, APF: adaptive power factor.

The proposed linear approximations in this work were briefly tested in our conference paper [33] for single-period deterministic AC OPF, on a small radial ADS and with a limited number of flexible options. These expressions are leveraged in this work to stochastic and multi-period AC OPF with a comprehensive set of flexible options and are validated on real-world larger, radial and weakly meshed, ADS to showcase its versatility and scalability. Moreover, we opt for devloping the proposed SLA for the following reasons. Linear approximations, in one step, of AC power flow or deterministic single-period AC OPF [29], [30], [31], [32] have been an extensive subject of research and used for a long time. This is mainly motivated by the fact that these equations are generally quadratic (when voltages are expressed in rectangular coordinates) and as such, they could be approximated reasonably well in a certain neighborhood of a linearization point. However, these single-shot approximations work well under normal operating conditions and restricted adjustments of decision variables around the point of linearization but might fail to work under stressed operating conditions or large number of adjustments of decision variables. To overcome such issues, distinct algorithms based on the concept of sequential linear programming [34], [35], [36] have been used for solving AC OPF problems. The ability of sequential linear programming to work well is based on the extensive knowledge and numerical experience gained in power systems for decades.

Finally, Table I summarizes the key features of the proposed framework, which distinguishes it from the existing works.

II. BENCHMARK STOCHASTIC MULTI-PERIOD AC-OPF MINLP FLEXIBILITY FRAMEWORK

This section presents the MINLP benchmark model for flexibility procurement through the S-MP-OPF framework in day-ahead operation planning of medium voltage ADSs. The model computes optimal schedules for flexible DER (RES, EESs, FLs) to be pursued for the next day to manage congestion or voltage issues [37]. The real-time operation control during

the next day may need to further minimize deviations from the day-ahead schedules but this is outside the scope of the paper.

Accordingly, the objective (1) minimizes the overall cost of network operation which consists of expected cost of DER re-dispatch from the market schedule (not shown explicitly for formulation ease) in each time period t and scenario s:

$$
\min \sum_{s \in S} \sum_{t \in T} \pi_s \Bigg\{ \Bigg(\sum_{i \in G} c_{i,p}^{curt} P_{i,s,t}^{curt} + \sum_{i \in B} c_{i,b}^{str} (P_{i,s,t}^{dch} - P_{i,s,t}^{ch})
$$
$$
+ c_{i,l}^{fl} \sum_{i \in F} (P_{i,s,t}^{od} + P_{i,s,t}^{ud}) \Bigg) \Delta T + c_{ij}^{oltc} \cdot \kappa_{if,s,t} \Bigg\} \quad (1)
$$

The problem obeys the following constraints ($\forall t \in T, s \in S$):

$$
P_{i,s,t}^e + (P_{i,s,t}^0 - P_{i,s,t}^{curt}) + (P_{i,s,t}^{dch} + P_{i,s,t}^{ch}) - (P_{i,s,t}^d + P_{i,s,t}^{od}
$$
$$
- P_{i,s,t}^{ud}) = \sum_{ij \in L \cup L^T} P_{ij,s,t} \qquad \forall i \in N \quad (2)
$$

$$
Q_{i,s,t}^e + Q_{i,s,t}^{RES} - \{Q_{i,s,t}^d + \tan(\varphi_{i,s,t})(P_{i,s,t}^{od} - P_{i,s,t}^{ud})\}
$$
$$
= \sum_{ij \in L \cup L^T} Q_{ij,s,t} \qquad \forall i \in N \quad (3)
$$

$$
P_{ij,s,t} = g_{ij} V_{i,s,t}^2 - g_{ij} V_{i,s,t} V_{j,s,t} \cos(\theta_{ij,s,t})
$$
$$
- b_{ij} V_{i,s,t} V_{j,s,t} \sin(\theta_{ij,s,t}) \qquad \forall ij \in L \cup L^T \quad (4)
$$

$$
Q_{ij,s,t} = -b_{ij} V_{i,s,t}^2 + b_{ij} V_{i,s,t} V_{j,s,t} \cos(\theta_{ij,s,t})
$$
$$
- g_{ij} V_{i,s,t} V_{j,s,t} \sin(\theta_{ij,s,t}) \qquad \forall ij \in L \cup L^T \quad (5)
$$

$$
\underline{V}_i^2 \leq V_i^2 \leq \overline{V}_i^2 \qquad \forall i \in N \quad (6)
$$

$$
(g_{ij}^2 + b_{ij}^2)\{V_{i,s,t}^2 + V_{j,s,t}^2 - 2V_{i,s,t} V_{j,s,t} \cos(\theta_{ij,s,t})\}
$$
$$
\leq |\overline{I}_{ij}|^2 \qquad \forall ij \in L \cup L^T \quad (7)
$$

$$
\underline{P}_i^e(\underline{Q}_i^e) \leq P_{i,s,t}^e(Q_{i,s,t}^e) \leq \overline{P}_i^e(\overline{Q}_i^e) \qquad \forall i \in E \quad (8)
$$

$$
0 \leq P_{g,s,t}^{curt} \leq P_{g,s,t}^0 \qquad \forall g \in G \quad (9)
$$

$$
-\tan(\overline{\phi}_{i,s,t})(P_{i,s,t}^0 - P_{i,s,t}^{curt}) \leq Q_{i,s,t}^{RES} \leq \tan(\overline{\phi}_{i,s,t})
$$
$$
(P_{i,s,t}^0 - P_{i,s,t}^{curt}) \qquad \forall i \in G \quad (10)
$$

$$
0 \leq P_{l,s,t}^{od} \leq M \cdot P_{l,s,t}^d \cdot \chi_{l,s,t}^{od} \qquad \forall l \in F \quad (11)
$$

$$
0 \leq P_{l,s,t}^{ud} \leq M \cdot P_{l,s,t}^d \cdot (1 - \chi_{l,s,t}^{od}) \qquad \forall l \in F \quad (12)
$$

$$
\sum_{t \in T} P_{l,s,t}^{od} \cdot \Delta T = \sum_{t \in T} P_{l,s,t}^{ud} \cdot \Delta T \qquad \forall l \in F \quad (13)
$$

$$
-\beta_{b,s,t}^{ch} \cdot P_b^{ch,r} \leq P_{b,s,t}^{ch} \leq 0 \qquad \forall b \in B \quad (14)
$$

$$
0 \leq P_{b,s,t}^{dch} \leq (1 - \beta_{b,s,t}^{ch}) \cdot P_b^{dch,r} \qquad \forall b \in B \quad (15)
$$

$$
SoC_{b,s,t} - SoC_{b,s,t-1} = \frac{\Delta T}{E_b^r} \left(-\eta_b^{ch} P_{b,s,t}^{ch} - \frac{P_{b,s,t}^{dch}}{\eta_b^{dch}} \right) \quad (16)
$$

$$
\underline{SoC}_b \leq SoC_{b,s,t} \leq \overline{SoC}_b \qquad \forall b \in B \quad (17)
$$

$$
SoC_{b,s,t_n} = SoC_{b,s,t_0} \qquad \forall b \in B \quad (18)
$$

$$
V_{f,s,t}^2 = \sum_{k=1}^Y r_{if}^k \times \lambda_{if,s,t}^k \qquad \forall if \in L^T, k \in Y \quad (19)
$$

$$
\underline{V}_i^2 \cdot \mu_{if,s,t}^k \leq \lambda_{if,s,t}^k \leq \overline{V}_i^2 \cdot \mu_{if,s,t}^k \qquad \forall if \in L^T, k \in Y \quad (20)
$$

$$
\underline{V}_i^2 \cdot (1 - \mu_{if,s,t}^k) \leq V_{i,s,t}^2 - \lambda_{if,s,t}^k \leq \overline{V}_i^2 \cdot (1 - \mu_{if,s,t}^k)
$$
$$
\forall if \in L^T, k \in Y \quad (21)
$$

$$
\sum_{k=1}^Y \mu_{if,s,t}^k = 1 \qquad \forall if \in L^T, k \in Y \quad (22)
$$

$$
|\sum_{k=1}^Y \{r_{if}^k \times \lambda_{if,s,t}^k\} - r_{if,s,t}^0| \leq \kappa_{if,s,t}
$$
$$
\forall if \in L^T, k \in Y \quad (23)
$$

where (2) and (3) are the active and reactive power balance constraints at each node, (4) and (5) are the active and reactive power flows through a branch, (6) is the limit on each bus voltage magnitude, (7) represents the longitudinal branch current limit, (8) limits the active (reactive) power flows at main substation, (9) and (10) model the active power curtailment and reactive power output of RES units, respectively, (11) and (12) limit the over- and under-demand of active power of FLs, (13) maintains the energy balance of FLs over whole horizon, (14) and (15) limit the active power charging and discharging of EESs, (16) models the EESs energy balance, (17) constraints the SoC and (18) maintains the SoC equal on the first and last time periods.

Eqs. (19)–(22) represent the model of an OLTC transformer as an ideal transformer in series with the transformer impedance. The introduction of a fictitious node (f) leads to $V_f^2 = r_{if}^2 V_i^2$, which is handled by the standard product of binary-continuous variables linearization approach [38], leading to constraints (19)–(22). Lastly, (23) models the transformer operation cost term in the objective function.

This MINLP formulation, termed hereafter M0, of S-MP-OPF framework, considers a comprehensive set of flexible options. However, in some ADSs, where FLs, EESs are not present and discreteness of OLTC is neglected, the problem reduces to a NLP model. Lastly, the intractability of M0 stems from binary variables as well as non-linear constraints (4)–(7). To ensure tractability, we develop an accurate approximation of this benchmark problem. To do so, the linear approximations of active and reactive power injections, and branch current expression are derived first in the Section IV.

III. ARIMA APPROACH FOR UNCERTAINTY MODELING

The uncertainty modeling of wind and PV DER is carried out through time-series based auto-regressive integrated moving average (ARIMA) approach, which is presented in detail in our paper [37]. However, for the sake of paper self containment, the modeling details are presented here as well.

The solar irradiance and wind speed, being non-stationary random process $Z(t)$, can be represented generically through ARIMA model (p, d, q) as follows [39]:

$$
\left\{1 - \sum_{i=1}^p \zeta_i B^i\right\} (1 - B)^d Z(t) = \left\{1 - \sum_{i=1}^q \varrho_i B^i\right\} \omega(t) \quad (24)
$$

where ζ_i and ϱ_i are auto-regressive and moving average terms, $\omega(t)$ is white noise having zero mean and variance υ^2, B is backshift operator such that $B^i Z(t) = Z(t - i)$.

The first step in the modeling process is to determine the values of (p, d, q) parameters and (ζ_i, ϱ_i) coefficients. The order d is determined by applying Augmented Dickey Fuller test on both solar and wind series. For q and p values, auto-correlation and partial auto-correlation functions are used for wind speed series. On the other hand, in the case of solar irradiance series, the order of p and q is set initially to 4 and then all those combinations of (p, q) are discarded for which ARIMA model polynomial becomes non-invertible. Finally, coefficients ζ_i and ϱ_i are determined using maximum likelihood estimation for Weibull distribution.

After determining the order (p, d, q) and (ζ_i, ϱ_i) coefficients, they are put in (24) to generate the solar power and wind speed scenarios. However, these scenarios are not the true representation of actual solar power and wind scenarios due to the presence of white noise term in (24). To nullify the effect of white noise in the generated scenarios, a distribution transformation process $Y(t) = \psi^{-1}\{F_z(Z)\}$ is carried out subsequently which generates the true scenarios of solar power and wind speed. In the mentioned transformation process, Z is the outcome of (24), F_z is the cumulative distribution function of Z and $\psi^{-1}()$ is the quantile (inverse distribution) function of the historical wind speed and solar power distribution. Lastly, wind speed scenarios are converted to wind power scenarios via Weibull speed-power transformation model [40].

IV. LINEARIZATION OF THE BENCHMARK MINLP MODEL

A. Linearized Active and Reactive Power Expressions

Let us first focus on the non-linear active and reactive power flows expressions in (4) and (5). It can be noticed that the non-linearity in (4) and (5) stems from the quadratic term (V_i^2), bi-linear term $(V_i V_j)$ and trigonometric terms $\{\cos(\theta_{ij}), \sin(\theta_{ij})\}$. Furthermore, voltage magnitude and angles are tightly coupled in $V_i V_j \cos(\theta_{ij})$ and $V_i V_j \sin(\theta_{ij})$ terms. The proposed approximation in this work tackles these non-linearities through the *second-order Taylor series* expansion of trigonometric terms and by transforming the bi-linear term into the square of voltage magnitude term. Resultantly, it introduces the *square of voltage magnitude* (V_i^2) and *voltage angle difference* (θ_{ij}) as new independent variables in order to transform (4) and (5) into approximate linear injections.

The proposed linearization procedure starts by substituting the trigonometric terms in (4) and (5) with their second-order Taylor series expansion terms around the initial linearization point $\theta_{ij}^{(0)}$, which leads to (the subscripts s and t are dropped in the following to ease the reading process):

$$P_{ij} = (g_{ij} + g_{ij}^{sh}/2)(V_i^2) - (c_1 g_{ij} + s_1 b_{ij})V_i V_j$$
$$- (c_2 g_{ij} + s_2 b_{ij})V_i V_j \theta_{ij} - (c_3 g_{ij} + s_3 b_{ij})V_i V_j \theta_{ij}^2 \tag{25}$$

$$Q_{ij} = -(b_{ij} + b_{ij}^{sh}/2)(V_i^2) + (c_1 b_{ij} - s_1 g_{ij})V_i V_j$$
$$+ (c_2 b_{ij} - s_2 g_{ij})V_i V_j \theta_{ij} + (c_3 b_{ij} - s_3 g_{ij})V_i V_j \theta_{ij}^2 \tag{26}$$

where $c_1 = s_2 + c_3 \theta_{ij}^{2(0)}$, $s_1 = -c_2 + s_3 \theta_{ij}^{2(0)}$, $c_2 = c^{(0)}\theta_{ij}^{(0)} - s^{(0)}$, $s_2 = s^{(0)}\theta_{ij}^{(0)} + c^{(0)}$, $c_3 = -\frac{c^{(0)}}{2}$, $s_3 = -\frac{s^{(0)}}{2}$, $c_0 = \cos(\theta_{ij}^{(0)})$ and $s_0 = \sin(\theta_{ij}^{(0)})$.

Eqs. (25) and (26) contain three non-linear terms $V_i V_j$, $V_i V_j \theta_{ij}$ and $V_i V_j \theta_{ij}^2$ where voltage magnitude and angles are still coupled in the last two terms. To decouple these terms, the second step involves the linearization of last two non-linear terms through the first-order Taylor series expansion.

1) Linearization of $V_i V_j \theta_{ij}$ and $V_i V_j \theta_{ij}^2$ Terms: By treating $V_i V_j$ and θ_{ij} as two independent terms, the first-order Taylor series expansion of $V_i V_j \theta_{ij}$ and $V_i V_j \theta_{ij}^2$ leads to:

$$V_i V_j \theta_{ij} \approx \theta_{ij}^{(0)}(V_i V_j) + V_i^{(0)} V_j^{(0)}(\theta_{ij} - \theta_{ij}^{(0)}) \tag{27}$$

$$V_i V_j \theta_{ij}^2 \approx \theta_{ij}^{2(0)}(V_i V_j) + 2V_i^{(0)} V_j^{(0)} \theta_{ij}^{(0)}(\theta_{ij} - \theta_{ij}^{(0)}) \tag{28}$$

Eqs. (27) and (28) show that the coupling between the voltages magnitude and angles no longer exist, and consequently, these expressions can be represented in terms of θ_{ij} variable. Furthermore, by substituting (27)-(28) in (25)-(26), the remaining non-linearity appears in $V_i V_j$ term.

2) Linearization of $V_i V_j$ Term: The approximation of non-convex bi-linear term $V_i V_j$ determines the accuracy of linearized active and reactive power injections, and consequently, the choice of methods for its linearization become crucial. In the majority of literature [29], [30], [31], [32], either $V_i V_j \approx 1$ approximation is used based on the assumption of flat/near-voltage profile or first-order Taylor series expansion of $V_i V_j$ is employed. However, these approximations no longer hold under distorted voltage profiles and stressed operating conditions. Consequently, in this paper, the following mathematical transformation is applied which leads to a more accurate linear representation of $V_i V_j$ term.

To express $V_i V_j$ in terms of V^2, we start from:

$$V_i V_j = \frac{V_i^2 + V_j^2}{2} - \frac{(V_i - V_j)^2}{2} = \frac{V_i^2 + V_j^2}{2} - \frac{(\Delta V_{ij})^2}{2} \tag{29}$$

The first fraction is linear in terms of V^2 and is capable of representing quite accurately the bi-linear term due to the fact that the second term involves the square of difference of voltage terms which, in general, is small provided the consecutive nodes voltages remain close to each other. However, under stressed operating conditions, this assumption may not hold and consequently, it becomes imperative to linearize ΔV_{ij}^2 as well. To do this, first it is written in terms of V^2 as shown in (30) and subsequently, its approximation via first-order Taylor series around initial operating point $V^{(0)}$ is carried out in (31).

$$\Delta V_{ij}^2 = \frac{(V_i + V_j)^2}{(V_i + V_j)^2}\Delta V_{ij}^2 \approx \frac{(V_i^2 - V_j^2)^2}{(V_i^{(0)} + V_j^{(0)})^2} \tag{30}$$

$$\Delta V_{ij}^2 \approx \frac{2(V_i^{(0)} - V_j^{(0)})(V_i^2 - V_j^2)}{(V_i^{(0)} + V_j^{(0)})} - (V_i^{(0)} - V_j^{(0)})^2 \tag{31}$$

TABLE II
COEFFICIENTS OF VARIABLES IN LINEARIZED ACTIVE & REACTIVE POWER FLOWS, AND LONGITUDINAL BRANCH CURRENT LIMIT EXPRESSION

Coefficients in P_{ij} (33)		Coefficients in Q_{ij} (34)		Coefficients in I_{ij} (36)	
$\alpha_{i,s,t}^{P}$	$p_1 \frac{(3V_{j,s,t}^{k-1}-V_{i,s,t}^{k-1})}{2(V_{i,s,t}^{k-1}+V_{j,s,t}^{k-1})}$	$\alpha_{i,s,t}^{Q}$	$-p_2 \frac{(3V_{j,s,t}^{k-1}-V_{i,s,t}^{k-1})}{2(V_{i,s,t}^{k-1}+V_{j,s,t}^{k-1})}$	$\alpha_{i,s,t}^{I}$	$\frac{c_1 V_{i,s,t}^{k-1}+c_2 V_{j,s,t}^{k-1}}{(V_{i,s,t}^{k-1}+V_{j,s,t}^{k-1})}$
$\alpha_{j,s,t}^{P}$	$p_1 \frac{(3V_{i,s,t}^{k-1}-V_{j,s,t}^{k-1})}{2(V_{i,s,t}^{k-1}+V_{j,s,t}^{k-1})}$	$\alpha_{j,s,t}^{Q}$	$-p_2 \frac{(3V_{i,s,t}^{k-1}-V_{j,s,t}^{k-1})}{2(V_{i,s,t}^{k-1}+V_{j,s,t}^{k-1})}$	$\alpha_{j,s,t}^{I}$	$\frac{c_2 V_{i,s,t}^{k-1}+c_1 V_{j,s,t}^{k-1}}{(V_{i,s,t}^{k-1}+V_{j,s,t}^{k-1})}$
$\beta_{ij,s,t}^{P}$	$p_2 V_{i,s,t}^{k-1} V_{j,s,t}^{k-1}$	$\beta_{ij,s,t}^{Q}$	$p_1 V_{i,s,t}^{k-1} V_{j,s,t}^{k-1}$	$\beta_{ij,s,t}^{I}$	$2s_{k-1} V_{i,s,t}^{k-1} V_{j,s,t}^{k-1}$
$\gamma_{i,s,t}^{P}$	$\{p_1 (V_{i,s,t}^{k-1}-V_{j,s,t}^{k-1})^2/2\}-$ $p_2 V_{i,s,t}^{k-1} V_{j,s,t}^{k-1} \theta_{ij,s,t}^{k-1}$	$\gamma_{i,s,t}^{Q}$	$\{-p_2 (V_{i,s,t}^{k-1}-V_{j,s,t}^{k-1})^2/2\}-$ $p_1 V_{i,s,t}^{k-1} V_{j,s,t}^{k-1} \theta_{ij,s,t}^{k-1}$	$\gamma_{i,s,t}^{I}$	$-2s_{k-1} V_{i,s,t}^{k-1} V_{j,s,t}^{k-1} \theta_{ij,s,t}^{(k-1)}-$ $c_{k-1}(V_{i,s,t}^{k-1}-V_{j,s,t}^{k-1})^2$

$p_1 = -c_{k-1}g_{ij} - s_{k-1}b_{ij}$; $p_2 = s_{k-1}g_{ij} - c_{k-1}b_{ij}$; $c_1 = 1 + c_{k-1}$; $c_2 = 1 - 3c_{k-1}$; k is the iteration number.

Substituting (31) into (29) leads to the linear representation of $V_i V_j$ in terms of V^2 as shown below.

$$V_i V_j \approx \frac{(V_i^2 + V_j^2)}{2} - (V_i^{(0)} - V_j^{(0)})^2 \left\{ \frac{(V_i^2 - V_j^2)}{(V_i^{2(0)} - V_j^{2(0)})} - \frac{1}{2} \right\} \tag{32}$$

In (32), (V^2, θ_{ij}) variable space is adopted (instead of (V, θ_{ij}) space) to reduce the overall linearization error, as it naturally captures more accurately the nonlinearity of terms involving voltage magnitudes. For instance, $g_{ij}^2 V_i^2$ and $b_{ij}^2 V_i^2$ terms become linear in (V^2, θ_{ij}) space and therefore the linearization of these terms is not required, which ultimately reduces the overall linearization error. On the other hand, the linearization of these terms is still required in (V, θ_{ij}) space.

3) Linearized Active and Reactive Power Expressions: Based on (27)-(28) and (32), the linearized active and reactive power flows in terms of V^2 and θ_{ij} become:

$$P_{ij} = \alpha_i^P V_i^2 + \alpha_j^P V_j^2 + \beta_{ij}^P \theta_{ij} + \gamma_i^P \tag{33}$$

$$Q_{ij} = \alpha_i^Q V_i^2 + \alpha_j^Q V_j^2 + \beta_{ij}^Q \theta_{ij} + \gamma_i^Q \tag{34}$$

where $\alpha_i^{P/Q}, \alpha_j^{P/Q}, \beta_{ij}^{P/Q}, \gamma^{P/Q}$ are the coefficients of V^2 and θ_{ij} variables, and are reported in Table II.

B. Linearized Longitudinal Branch Current Expression

The thermal loading on a branch ij can be expressed as:

$$|I_{ij}|^2 = (g_{ij}^2 + b_{ij}^2)\{V_i^2 + V_j^2 - 2V_i V_j \cos(\theta_{ij})\} \tag{35}$$

which is non-linear due to V^2 and $V_i V_j \cos(\theta_{ij})$ terms. As stated earlier, the latter term can be linearized, in terms of V^2, through second-order Taylor series expansion of cosine term and subsequently, using (32), which ultimately leads to:

$$|I_{ij}|^2 = (g_{ij}^2 + b_{ij}^2)(\alpha_i^I V_i^2 + \alpha_j^I V_j^2 + \beta_{ij}^I \theta_{ij} + \gamma_i^I) \tag{36}$$

where $\alpha_i^I, \alpha_j^I, \beta_{ij}^I, \gamma^I$ are the coefficients of V^2 and θ_{ij} variables and are reported in Table II.

Note that in Table II, the coefficients are reported for expressions under a stochastic multi-period framework i.e., parameters are derived for each scenario s and time period t. Furthermore, the parameter k represents either the inner- or outer-loop iteration of the sequential linearization algorithm, and V^k and θ^k

represent the values of voltage magnitude and angle difference recovered in iteration k.

Finally, the presented linear expressions in this section clear the pathway towards a tractable model under S-MP-OPF framework which is presented in the next section.

V. PROPOSED TRACTABLE METHODOLOGY

The proposed tractable methodology consists of the derived linear-expressions, a mixed-integer linear programming (MILP) model, termed M1, based on these expressions and the sequential linearization algorithm (SLA) which incorporates M1. Hereafter, both M1 and SLA are described in detail.

A. MILP Model Under S-MP-OPF Flexibility Procurement Framework

The proposed model (M1) is expressed in V^2 and θ_{ij}; it minimizes (1) and obeys (2)–(3), (6), (8)–(23) and (37)–(43).

$$P_{ij,s,t} = \alpha_{i,s,t}^p V_{i,s,t}^2 + \alpha_{j,s,t}^p V_{j,s,t}^2 + \beta_{ij,s,t}^p \theta_{ij,s,t} + \gamma_{i,s,t}^p$$
$$\forall ij \in L \tag{37}$$

$$Q_{ij,s,t} = \alpha_{i,s,t}^q V_{i,s,t}^2 + \alpha_{j,s,t}^q V_{j,s,t}^2 + \beta_{ij,s,t}^q \theta_{ij,s,t} + \gamma_{i,s,t}^q$$
$$\forall ij \in L \tag{38}$$

$$P_{fj,s,t} = \alpha_{f,s,t}^p V_{f,s,t}^2 + \alpha_{j,s,t}^p V_{j,s,t}^2 + \beta_{fj,s,t}^p \theta_{fj,s,t} + \gamma_{f,s,t}^p$$
$$\forall fj \in L^T \tag{39}$$

$$Q_{fj,s,t} = \alpha_{f,s,t}^q V_{f,s,t}^2 + \alpha_{j,s,t}^q V_{j,s,t}^2 + \beta_{fj,s,t}^q \theta_{fj,s,t} + \gamma_{f,s,t}^q$$
$$\forall fj \in L^T \tag{40}$$

$$(g_{ij}^2 + b_{ij}^2)(\alpha_{i,s,t}^I V_{i,s,t}^2 + \alpha_{j,s,t}^I V_{j,s,t}^2 + \beta_{ij,s,t}^I \theta_{ij,s,t} + \gamma_{i,s,t}^I)$$
$$\leq |I_{ij}|^2 \qquad \forall ij \in L \tag{41}$$

$$\underline{\theta}_{ij,s,t} \leq \theta_{ij,s,t} \leq \overline{\theta}_{ij,s,t} \qquad \forall ij \in L \cup L^T \tag{42}$$

$$\rho_{i,s,t}(V_{i,s,t}^2 + V_{j,s,t}^2) - \upsilon_{i,s,t}(V_{i,s,t}^2 - V_{j,s,t}^2) + \xi_{i,s,t} \geq 0$$
$$\forall i, j \in N \tag{43}$$

where (37)-(38) and (39)-(40) represent the linear active and reactive power flows through a line and transformer, respectively, (41) models the linear branch current expression, (42)

restricts the difference of voltage angles within defined bounds and (43) ensures the positivity of ΔV_{ij}^2, where coefficients in (43) are defined as $\rho_{i,s,t} = 1/2, \upsilon_{i,s,t} = \frac{V_{i,s,t}^{2^{(0)}} - V_{j,s,t}^{2^{(0)}}}{V_{i,s,t}^{2^{(0)}} + V_{j,s,t}^{2^{(0)}}}, \xi_{i,s,t} = (V_{i,s,t}^{2^{(0)}} - V_{j,s,t}^{2^{(0)}})^2/2$.

The presented model M1 is valid for radial distribution systems only. In order to make it applicable for meshed systems, we propose to extend it with the following constraint.

$$\sum_{ij \in L^c} \theta_{ij,s,t} = 2n\pi \qquad \forall ij \in L^c \qquad (44)$$

where (44) ensures the cyclic angle constraint (i.e., summation of voltage angle differences over each cycle in a mesh is zero).

Finally, as briefly mentioned in Section I, linear active and reactive power flow expressions in (V^2, θ_{ij}) variables space are proposed in [29] as well. However, due to small angle and near/flat voltage profile assumptions, $V_i V_j \theta_{ij}$ term is simply reduced to θ_{ij} term and $V_i V_j \theta_{ij}^2$ term does not appear in [29]. Resultantly, the coefficients of V^2 and θ_{ij} variables as well as constant terms in the active and reactive power injection terms are completely different in our work (presented in Table II) than in [29]. Moreover, the linearized branch current expressions (41) in (V^2, θ_{ij}) variable space are derived for the first time in this work. Lastly, we have thoroughly validated the performance of our proposed methodology under a complex and challenging S-MP-OPF framework, whereas expressions in [29] are tested only for deterministic single period OPF. We have compared our proposed methodology against the model [29] in Section V.

B. Trustable Approximation Criterion

The normalized relative difference between the non-linear apparent power injection S^{nl} (determined by injecting the solution of model M1 in (4) and (5)) and its linear estimation S^{lin} at each node, calculated over the whole time horizon and uncertainty scenarios, is chosen as the trustable approximation criterion (45). This will evaluate the accuracy of the proposed model M1 solution in the inner-loop of SLA as shown later.

$$\Delta S_i = \max \left\{ \frac{\sum\limits_{s \in S} \sum\limits_{t \in T} S_{s,t,i}^{nl} - \sum\limits_{s \in S} \sum\limits_{t \in T} S_{s,t,i}^{lin}}{S \times T \times \max\left(\sum\limits_{s \in S} \sum\limits_{t \in T} S_{s,t,i}^{nl}\right)} \right\} \quad \forall i \in N \qquad (45)$$

The satisfaction of approximation criterion ($\Delta S_i \le \epsilon, \forall i \in N$) ensures that the probability of the obtained M1 solution to lie in the close vicinity of the benchmark M0 solution is high. Resultantly, the optimality gap (difference between the optimal solutions of M0 and M1) can be zero or negligible. However, note that the satisfaction of this criterion does not guarantee that the obtained solution is AC feasible; this needs to be further verified by plugging the value of control variables obtained from M1 in the AC power flow (PF), as explained hereafter.

C. Sequential Linearization Algorithm

To solve the benchmark model M0, with high accuracy, we propose the SLA shown in the Fig. 1. The algorithm hinges on
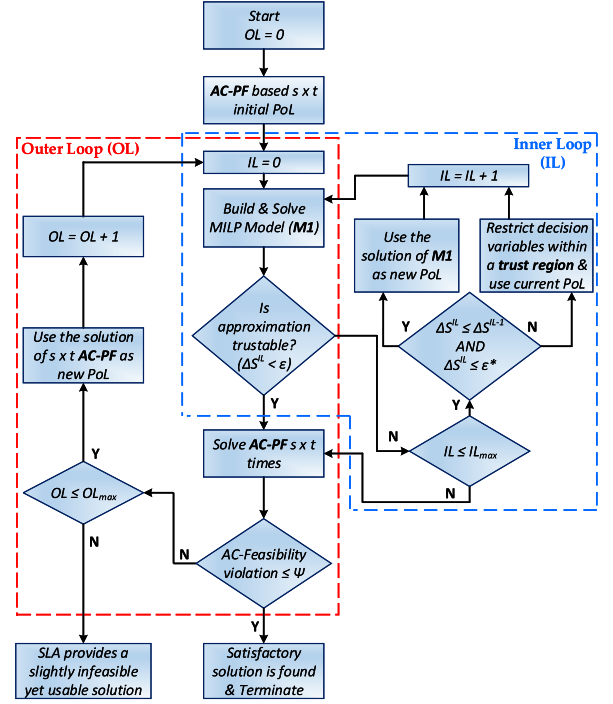

Fig. 1. Flow chart of the proposed sequential linearization algorithm.

the empirical assumption that, given the significant number of integer variables in the benchmark model M0, solving a reduced number of times the model M1 (in practice a few) is much faster computationally and scalable than solving the model M0. The steps of SLA are as follows.

1) Run AC PF $s \times t$ times to obtain the *initial* point-of-linearization (PoL) in each scenario s/time-period t.
2) Calculate the coefficients of linearized active and reactive power injections, and branch current expressions, as reported in Table II, using the initial PoL.
3) Build and solve the model M1 around the current PoL.
4) Evaluate the trustable approximation criterion. If it is satisfied, go to step 7.
5) Update PoL based upon the value of trustable approximation criterion in the current inner-loop iteration i.e., either update PoL greedily[1] by the recovered solution (voltage magnitude and angle) of model M1 or keep it the same in the next iteration if divergence in the model M1 solution, with respect to the previous inner-loop iteration, is detected (for more detailed explanation of the last point, please see Section V-C1).
6) Go to step 3 i.e., build and solve model M1 around the updated PoL.
7) Check the AC feasibility of the recovered approximated OPF (model M1) solution. If no constraints (voltage magnitude and branch loading limits) are violated, the algorithm terminates.

---

[1]Note that the updated PoL is not obtained by a PF solution but rather, model M1 solution simply *estimates* the power flow solution.

8) Update the PoL in each scenario s and time-period t by AC PF solution (voltage magnitude and angle) determined in the outer loop, and go to step 3.

1) Role of Inner- and Outer-Loops: The proposed heuristic SLA consists of inner- and outer-loops as shown in Fig. 1.

The objective of the inner-loop is to ensure the convergence of proposed model M1 by properly updating the PoL based on the value of trustable approximation criterion in the current inner-loop iteration.

It can be noticed that if criteria $\Delta S_i^{IL} < \Delta S_i^{IL-1}$ and $\Delta S_i \leq \epsilon^*, \forall i \in N$, where $\epsilon^* > \epsilon$, are satisfied, it means that model M1 solution lies in the close vicinity of the optimal solution, and as such one can greedily update the PoL by using model M1 solution as a new PoL. Hence, the necessity of computing a new PoL through $s \times t$ AC PF is avoided and the *estimated* AC PF solution (nodes voltage magnitude and angles are recovered from model M1 and are not determined by running $s \times t$ AC PF; thus the recovered solution is termed as estimated AC PF solution) is used as a new PoL.

On the other hand, if the above-mentioned criteria $\Delta S_i^{IL} < \Delta S_i^{IL-1}$ and $\Delta S_i \leq \epsilon^*, \forall i \in N$ are not satisfied, it means that model M1 solution either moves towards the optimal solution but still far from it i.e., ($\Delta S_i^{IL} < \Delta S_i^{IL-1}$ but $\Delta S_i > \epsilon^*$) or it starts moving away from the optimal solution i.e., ($\Delta S_i^{IL} > \Delta S_i^{IL-1}$). Under both circumstances, the decision variables are restricted within a trust region, model M1 is solved again at the current PoL (or the best encountered solution in previous iterations can be used as a new PoL), which is updated, at the solution of model M1, in the subsequent inner-loop iteration.

The role of outer-loop is to determine the AC feasibility of the computed model M1 solution once trustable approximation criterion is satisfied in the inner-loop. This means that if all constraints (voltage magnitude and branch overload) are either satisfied or below the chosen feasibility threshold at the obtained model M1 solution, an AC feasible solution has been provided by the model M1 and, resultantly, SLA terminates. On the other hand, if constraints violate the feasibility threshold, the outer-loop updates the PoL at the solution of AC PF and model M1 is solved again around the new PoL in the next inner-loop iteration.

2) Remarks About the Point of Linearization: The proposed SLA relies on two AC PF modules for the PoL. The first AC PF module, which is outside the inner- and outer-loops, provides the *initial* PoL, whereas the second AC PF module is in the outer-loop and it updates the PoL after checking the AC feasibility of recovered model M1 solution.

Note that during the calculation of the *initial* PoL, only RES available active power in each scenario s over the whole-horizon are considered in the AC PF (for reactive power of RES, a power factor of 0.9 is considered; however, any value of power factor can be chosen based upon the grid-code of a particular country). Furthermore, the values of control variables (RES curtailment, EESs active power charging and discharging, over/under-demand of active power of FLs) are set to zero except transformer tap-ratio which is set to 1, as this information is not known beforehand and can only become available once model M1 is solved. Consequently, the quality of the initial $s \times t$

TABLE III
INSTALLED DER AND PEAK LOAD DEMAND IN THE THREE TEST CASES

Test Cases	RES		EESs		FLs+	Peak Load	
	No.	Cap. (MW)	No.	Cap. (MW)	No.	P (MW)	Q (MVAr)
34-bus	8	0.5/1	3	1	2	3.71	2.30
UK 31-bus	8	2.6	3	1	4	6.51	2.14
PT. 191-bus	23	2.0	10	1	20	18.75	6.16

Cap: Capacity is defined per DER.
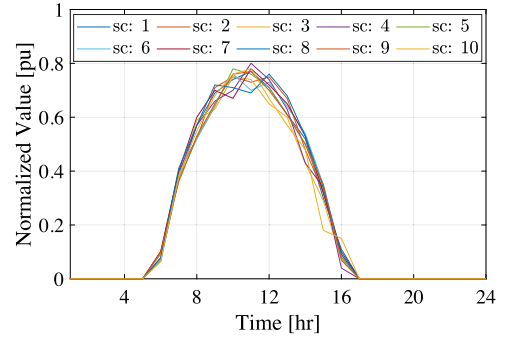+ Flexibility from each FL is taken as 50% of its total demand.

Fig. 2.   PV scenarios.

PoL may be affected; depending on the number and values of RES, EESs, FLs and OLTC transformers. Nevertheless, in the presence of more refined information such as data from local energy markets in the future, DSOs will have access to more precise settings of all these resources, which will improve the quality of initial PoL.

During subsequent outer-loop iterations, the values of control variables become available, after model M1 is solved, and thus are utilized while determining the new $s \times t$ PoL in the second AC PF module. Consequently, the quality of PoL and, in turn, the accuracy of model M1 is improved remarkably.

VI. NUMERICAL RESULTS

A. Test Networks and General Assumptions

The proposed SLA is tested on the modified version of following three test systems (i) 34-bus 12.66 kV radial ADS (see Fig. 4) [37], (ii) 30-bus 11 kV weakly-meshed real U.K. ADS [41] and (iii) 191-bus 30 kV radial real Portuguese ADS [41]. In the context of flexibility provision framework, DER rich versions of these networks are considered. Table III shows the numbers and capacities of DER considered in these systems. Finally, the bench-marking of SLA is carried out using the 34-bus ADS, whereas its scalability and performance on ADSs with different characteristics (e.g., weakly meshed) is shown through the U.K. and Portuguese ADSs.

The simulations are performed for 24 time-periods (an hourly resolution is considered which is reasonable for day-ahead operation planning framework) using, without loss of generality, 10 uncertainty scenarios of solar and wind DER, which are generated through ARIMA model. Figs. 2 and 3 show the generated representative scenarios for solar PV and wind DER,
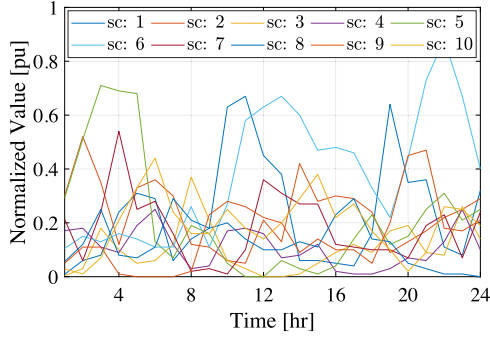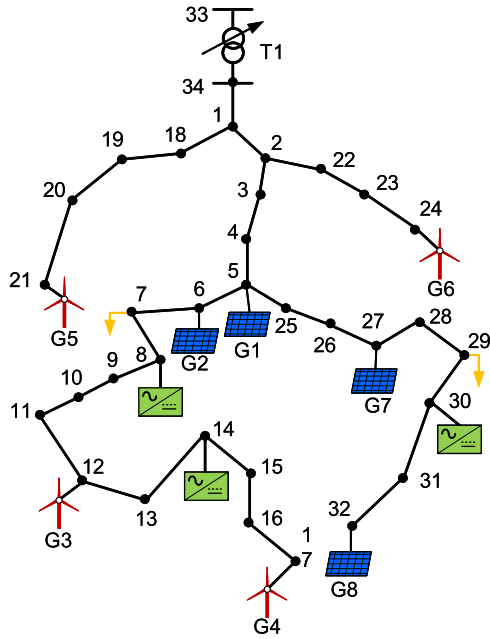
Fig. 3. Wind scenarios.

Fig. 4. Layout of modified 34-bus distribution network.

The AC feasibility threshold (ψ) is set to 1% i.e., the value of nodes voltages and/or branch current above 1% of their rated pu values is considered as an infeasible solution. Lastly, both benchmark and SLA are developed in Julia/JuMP [42] and are solved using Bonmin (with modified settings: ratio gap = 0.05, allowable gap = 0.01) and CPLEX solvers, respectively.

B. Flexibility Options

The proposed flexibility framework is studied for nine different combinations of flexible options (FOs), termed as FO1-FO9, to evaluate the proposed SLA under different operating conditions. These FOs are active power curtailment (APC-FO1) and various combinations of APC with (i) OLTC transformer (FO2), (ii) adaptive power factor (APF-FO3), (iii) OLTC and APF (FO4), (iv) EESs (FO5), (v) FLs (FO6), (vi) EESs and FLs (FO7), (vii) EESs, FLs and APF (FO8) and (viii) EESs, FLs, APF and OLTC (FO9). For FOs involving APF, the power factor of each RES unit varies between 0.90 lagging and 0.90 leading. Finally, under FOs 1 and 3, models M0 and M1 reduce to NLP and LP models, respectively due to lack of integer variables.

C. Results for 34-Bus Test System

To test the accuracy of proposed SLA under hard conditions, a highly stressed operating point was created on purpose. For example, the total number of *initial* voltage violations, before solving the SLA, is 541 where 310 violations are above the feasibility threshold ($\psi > 1\%$) and the maximum observed violation is 12.4% above the upper voltage limit.

1) Evaluating the Accuracy of the Proposed SLA: Table IV shows the performance of proposed SLA by comparing the obtained results with the solution of model M0 in terms of optimality gap and computational time. The optimality gap is defined as $\left| \frac{M0^{obj} - M1^{obj}}{M0^{obj}} \right|$ where $M0^{obj}/M1^{obj}$ is the optimal solution obtained after solving model M0/proposed SLA. The smaller the value of optimality gap, the closer the solution of proposed SLA to the benchmark optimal solution. It can be noticed that under all FOs, the optimality gap is much less than 1%; especially, in FOs 1-7, the gap is almost zero. This shows that the proposed SLA converges to the same optimal solution as model M0 and, as such, it is capable of achieving excellent accuracy.

In terms of SLA convergence, it is observed that in all cases, SLA takes two inner-loop iterations and one outer-loop pass to satisfy the trustable approximation (ϵ) and feasibility threshold (ψ) criteria, respectively. In terms of AC feasibility of SLA converged solution (shown in the constraints violations column), the maximum violation for each FO is negligible (e.g., roughly 2×10^{-6} pu) and almost 1000 times smaller than the feasibility threshold ($\psi \leq 1\%$). Accordingly, the monitored violations are rather numerical errors in the range of solver convergence tolerance than actual violations. Furthermore, the trustable approximation criterion is satisfied in all FOs with its value varying between 1.12 VA (FO1) - 370 VA (FO5).

2) Computational Performance: From problem statistics point-of-view, it can noticed that both models contain almost

respectively. It can be seen that the output active power of wind DER varies significantly across different scenarios, while it shows less variability in the case of PV DER. This is mainly due to the fact that the chosen one-year solar irradiance data for generating PV scenarios do not show too much variation over the whole year. Furthermore, the reduced geographical span of an ADS accounts for the scenarios proximity. However, the proposed tractable methodology can accommodate any type of scenarios i.e., similar or distinct, and can provide the output results, provided the developed model M1 remains feasible. Albeit there exists sophisticated uncertainty modeling methods, they are impractical for large scale real-world ADSs leading to unmanageable problems. Consequently, we accommodate a reasonable number of sampled scenarios in the proposed S-MP-OPF framework.

The maximum inner-loop ($IL_{\max}$) and outer-loop ($OL_{\max}$) iterations are set to 3 and 5, respectively. The trustable approximation criterion (ϵ) is set to 1×10^{-3} pu in order to restrict the error value, i.e., (45), below 1 kVA in all test cases. The ϵ^* is set to 1×10^{-1} pu to switch to trust region path in the inner-loop.

TABLE IV
PERFORMANCE OF PROPOSED SLA IN 34-BUS ADS AND COMPARISON WITH THE BENCHMARK MINLP MODEL

FOs	Optimality Gap (%)	Constraints Violations*			IL Approximation Error		SLA Iter.		Problem Statistics and Computational Time							
		No.	Max (%)	≤ 1%	Max Error (pu)	Mean Error (pu)	IL	OL	Model M0				Model M1			SLA
									BV	CV	CSTR	Time	BV	CV	CSTR	Time
FO 1	0.05	0	2.60×10^{-4}	0	1.1×10^{-5}	2.9×10^{-8}	2	1	0	18720	35040	16.4	0	19200	58800	3.2
FO 2	0.02	0	2.53×10^{-4}	0	8.6×10^{-6}	1.9×10^{-6}	2	1	2160	19200	36000	3600*	2160	20880	66000	13.3
FO 3	0.07	0	2.61×10^{-4}	0	5.1×10^{-6}	2.5×10^{-7}	2	1	0	20640	40800	20.9	0	21120	64560	3.0
FO 4	0.06	0	2.54×10^{-4}	0	2.0×10^{-5}	4.9×10^{-6}	2	1	2160	21120	41760	3600*	2160	22800	71760	16.3
FO 5	0.03	0	2.60×10^{-4}	0	3.7×10^{-4}	1.5×10^{-5}	2	1	720	21600	38640	94.3	720	22080	65010	11.8
FO 6	0.03	0	2.60×10^{-4}	0	1.4×10^{-5}	5.9×10^{-7}	2	1	480	19680	36020	33.7	480	20160	61220	9.8
FO 7	0.02	0	2.32×10^{-4}	0	2.3×10^{-4}	9.1×10^{-6}	2	1	1200	22560	39620	93.4	1200	23040	66980	13.9
FO 8	0.23	0	2.58×10^{-4}	0	2.6×10^{-5}	1.4×10^{-6}	2	1	1200	24480	45140	71.6	1200	24960	72740	17.0
FO 9	0.26	0	2.60×10^{-4}	0	3.5×10^{-5}	4.9×10^{-6}	2	1	3360	24960	46100	3600*	3360	26640	79940	23.1

Iter. = iteration; CSTR = constraints; CV = continuous variable; BV = binary variable; IL = inner loop; OL = outer loop;
*: maximum time execution limit reached in MINLP solver.
⋆: Only voltage violations are reported in Table IV as branch current limits are satisfied in all FOs.

the same number of variables. However, model M1 contains roughly 50-80% more constraints than model M0.

Despite being larger in size, the proposed SLA is considerably faster than M0 in all FOs. For example, in FOs 1 and 3, SLA takes almost 3 seconds to reach an optimum and is 5–7 times faster than M0, mainly because of the LP nature of model M1 in these FOs. Similarly for FOs 5-8 where both models consider OLTC ratio as a parameter, the computational time of proposed SLA is 3-8 times shorter than the solution time of model M0. Finally, for FOs in which OLTC ratio is treated as a variable (FOs 2, 4 and 9), model M0 reaches the maximum time execution constraint, which is set to 3600 seconds. Moreover, the MINLP solver did not return even an integer solution when the computation was aborted and provides only a utopian lower bound. On the contrary, the proposed SLA provides the optimal and feasible solution in less than 30 seconds for all such FOs.

From now on, the scalability and the versatility of presented SLA (and model M1) is demonstrated on two real-world ADSs for a reduced number of flexible options.

D. Results for 30-Bus Weakly-Meshed U.k. Test System

The proposed SLA is tested for the following two cases (i) base case (original limits) and (ii) stressed operating conditions (thermal limit is reduced on three branches by 20%). This ADS is initially congested during 17 and 24 instances in these cases, respectively and the maximum overload value is 44.8% above the rated thermal limit in both cases. Additionally, no voltage violations are observed in these cases.

Finally, FOs 4 and 9 are studied for two sets of taps, having 9 and 17 number of taps, to evaluate the proposed SLA.

1) Base Case: The following observations can be made from the presented results in Table V. In terms of solution accuracy, both model M0 and proposed SLA converge to the almost same solution as optimality gap stays below 0.21% in all FOs. The AC feasible solution is obtained in just one outer-loop iteration as well as the branch current limits are satisfied in all FOs and no overload instance is observed.

Regarding computational efficiency, the presented SLA outperforms the benchmark model M0 in all FOs. In FOs 1, 7 and

TABLE V
BASE CASE: 31-BUS WEAKLY-MESHED U.K. ADS

FOs	Optimality Gap (%)	Constraints Violations					Iter. IL/OL	Time (s)	
		No.	Max (%)	Avg (%)	≤Avg	≤1%		M0	SLA
FO 1	0.03	0	0	0	0	0	2/1	31	1
FO 4†	0.00	0	0	0	0	0	3/1	3600*	23
FO 4‡	0.18	0	0	0	0	0	2/1	3600*	5
FO 7	0.21	0	0	0	0	0	3/1	82	6
FO 8	0.21	0	0	0	0	0	3/1	167	11
FO 9†	0.01	0	0	0	0	0	3/1	3600*	20
FO 9‡	0.01	0	0	0	0	0	2/1	3600*	8

†: taps = 09 ‡: taps = 17; IL = inner loop; OL = outer loop.

TABLE VI
STRESSED CASE: 31-BUS WEAKLY-MESHED U.K. ADS

FOs	Optimality Gap (%)	Constraints Violations					Iter. IL/OL	Time (s)	
		No.	Max (%)	Avg (%)	≤Avg	≤1%		M0	SLA
FO 1	0.00	4	0.38	0.15	3	4	2/1	31	1
FO 4†	0.00	9	0.22	0.13	4	9	3/1	3600*	20
FO 4‡	0.14	4	0.04	0.02	2	4	2/1	3600*	6
FO 7	0.14	8	0.71	0.17	6	8	3/1	142	6
FO 8	0.14	8	0.55	0.13	6	8	3/1	119	9
FO 9†	0.05	2	0.01	0.003	1	2	2/2	3600*	28
FO 9‡	0.05	9	0.10	0.02	6	9	2/2	3600*	21

†: taps = 09 ‡: taps = 17; IL = inner loop; OL = outer loop.

8, the model M0 is 13-30 times slower than the proposed SLA, whereas it hits the maximum solution time limit (3600 seconds) in FOs 4 and 9 under both number of taps and provides only a utopian lower bound on the optimal value. The proposed SLA provides a feasible solution in almost 25 seconds (extremely faster than M0) for both FOs and taps.

2) Robustness Under Stressed Operating Conditions: From the presented results in Table VI, it can be noticed again that a highly accurate solution is provided by SLA in all FOs as maximum optimality gap is merely 0.14%. The AC feasible solution is obtained in one outer-loop iteration in all FOs except FO9 (under 9 and 17 taps), which requires two outer-loop iterations to reach an AC feasible solution.

In contrast to the base case, it is observed that overload instances exist in all FOs. However, as feasibility threshold is not violated in any of the overload instances, the obtained SLA solution is treated as a feasible solution in this work

TABLE VII
BASE CASE: 191-BUS RADIAL PORTUGUESE ADS

FOs	Optimality Gap (%)	Constraints Violations					Iter. IL/OL	Time (s)	
		No.	Max (%)	Avg (%)	≤Avg	≤1%		M0	SLA
FO 1	0.01	0	0.00	0.00	0	0	2/1	451	26
FO 4†	0.01	1	0.18	0.18	0	1	3/1	3600*	48
FO 4‡	0.05	1	0.60	0.60	0	1	3/1	3600*	53
FO 7	0.19	4	0.02	0.01	2	4	3/1	3600*	44
FO 9†	0.00	3	0.01	0.01	2	3	3/1	3600*	209
FO 9‡	0.00	1	0.13	0.13	0	1	3/1	3600*	168

†: taps = 09 ‡: taps = 17; IL = inner loop; OL = outer loop.
*: maximum time execution limit reached in MINLP solver.

TABLE VIII
STRESSED CASE: 191-BUS RADIAL PORTUGUESE ADS

FOs	Optimality Gap (%)	Constraints Violations					Iter. IL/OL	Time (s)	
		No.	Max (%)	Avg (%)	≤Avg	≤1%		M0	SLA
FO 1	0.01	16	0.64	0.13	14	16	2/1	429	25
FO 4†	0.01	3	0.37	0.05	0	1	3/2	3600*	254
FO 4‡	0.01	17	0.80	0.09	15	17	3/1	3600*	97
FO 7	0.07	15	**1.14**	0.08	14	14	3/5	3600*	323
FO 9†	0.03	11	0.03	0.003	2	3	3/1	3600*	234
FO 9‡	0.04	13	0.10	0.02	4	13	3/1	3600*	270

†: taps = 09 ‡: taps = 17; IL = inner loop; OL = outer loop.
*: maximum time execution limit reached in MINLP/MILP solver.

TABLE IX
PROPOSED SLA SCALABILITY TEST UNDER INCREASING NUMBER OF SCENARIOS AND TIME-PERIODS

Sc.	24 time-periods				96 time-periods			
	BV	CV	CSTR	Time	BV	CV	CSTR	Time
	(k)	(M)		(s)	(k)	(M)		(s)
10	11.3	126.7	0.39	168	45.1	507	1.57	1511
20	22.6	253.4	0.79	358	90.2	101.3	3.14	8904
30	33.8	380.2	1.18	793	135.3	152.1	4.71	10849
40	45.1	506.8	1.57	1419	180.4	203	6.29	OoM*
50	56.4	633.6	1.96	3374	225.6	253	7.86	OoM*

Sc. = Number of Scenarios; BV = binary variable; CV = continuous variable; CSTR = constraints; k = thousand; M = Million; OoM = Out-of-Memory.

(further analysis and discussion is provided in Section VI-G). For example, in FO7, 8 instances goes above the thermal limit; however, the maximum overload value is 0.71%, whereas the average overload value is 0.17% and the majority of overload instances (6 out of 8) are below the average value (a similar trend is noticed in the other FOs).

In terms of computational time, the proposed SLA is 13-30 times faster (similar to the base case) than M0 in FOs 1, 7 and 8. For the remaining FOs, it returns an optimal solution under 30 seconds and, thus outperforms M0 computationally.

E. Results for 191-Bus Portuguese Test System

The scalability of proposed SLA is tested and shown in Tables VII-VIII for two cases (i) base case (original limits) and (ii) stressed operating conditions (thermal limit is reduced on 8 branches by 20%). This ADS is also initially congested during 6 and 27 instances in these cases, respectively. Moreover, the maximum overload values are 11% and 36% above the rated limit in these cases.

1) Base Case: The presented results in Table VII shows that the proposed SLA almost provides the same solution as obtained from model M0, as the optimality gap stays less than 0.10% in all FOs except FO7, where error becomes 0.19%.

A couple of overload instances are observed in all FOs (except FO1); however, the maximum overload values stay within the feasibility threshold (in fact the maximum overload value, observed in FO4‡, is merely 0.60%).

Regarding computational efficiency, MINLP fails to solve M0 within the allotted time in all FOs except FO1 (no binary variable) and provides only a utopian lower bound. The SLA, on the other hand, is significantly faster than M0 in all FOs. For instance, in FOs 1, 4†, 4‡ and 7, the solution time remains below 1 minute, whereas for FOs 9† and 9‡, the optimal solution is obtained within 3-4 minutes. These results clearly show that the

proposed SLA is capable of providing a highly accurate solution within few minutes for large real-world ADS.

2) Robustness Under Stressed Operating Conditions: From the presented results in Table VIII, it can be noticed that the optimality gap in all FOs remains below 0.10%. Resultantly, SLA leads to the same solution as provided by model M0. Furthermore, AC feasible solution is obtained in one outer-loop iteration in all FOs except FOs 4† which need one more iteration to reach to an AC feasible solution.

Although few overload instances are observed in all FOs, no overload instance, except one in FO7, violates the feasibility threshold. In FO7, one instance is above the feasibility threshold; however, the violation value is merely 0.14%. Moreover, the number of congested instances as well as peak overload values are reduced drastically as compared to the initial number of congested instances. Accordingly, the obtained solution in FO7, albeit slightly infeasible, can still be used by DSOs.

Regarding computational efficiency, the solution time is 1.2 (FO 9†) to 7.34 (FO 4†) times larger than the solution time of the base case. Nevertheless, AC feasible solution is obtained in all FOs within 1–6 minutes. In contrast, the benchmark model M0 fails to converge within the allotted time in all FOs except FO1. These results clearly indicate that a highly accurate workable solution can be achieved by the proposed SLA, which seems, otherwise, almost impossible to obtain using benchmark model M0 in a reasonable amount of time.

F. Further Scalability Tests

Table IX explores further the scalability of proposed SLA for increasing number of scenarios and time-periods (the two main factors affecting the problem size) for PT-191 bus ADS in FO9‡. Note that solution time increases more than linearly with the problem size. For instance, the problem size increases by 5 times from 10 to 50 scenarios under 24 time-periods while the solution time grows 19 times.

One can safely conclude that the computation time is moderate and hence compatible with the day-ahead operation application (i.e., less than one hour) for a problem which is 5 times larger (50 scenarios and 24 time-periods) than the base case (10 scenarios and 24 time-periods). Beyond this problem size, the optimal solution is obtained approximately in 2-3 hours (scenarios 20-30 under 96 time-periods), which could be deemed still acceptable in day-ahead operation planning. However, for scenarios 40 and

TABLE X
PERFORMANCE OF LINEARIZATION METHODOLOGY [29] FOR S-MP OPF

FOs	Optimality Gap (%)	Constraints Violations					Iter. IL/OL	Time (s)	
		No.	Max (%)	Avg (%)	$\leq$Avg	$\leq$1%		SLA	[29]
FO 1	0.02	15	0.64	0.12	12	15	2/2	25	32
FO 4†	0.04	10	**3.44**	0.77	5	9	3/5	254	474
FO 4‡	0.03	10	**10.5**	3.02	7	6	3/5	97	198
FO 7	0.06	11	0.23	0.09	7	11	3/2	323	39
FO 9†	0.08	6	**1.08**	0.62	2	5	3/5	234	383
FO 9‡	0.07	6	0.61	0.11	5	6	3/4	270	342

$\dagger$: taps = 09 $\ddagger$: taps = 17; IL = inner loop; OL = outer loop.
*: maximum time execution limit reached in MINLP/MILP solver.

50 in 96 time-periods, CPLEX runs out-of-memory during the first inner-loop iteration, and, as such, is unable to provide the solution.

Based on these results, it can be extrapolated that the proposed SLA is scalable to ADSs which are at least 4-5 times larger (800–1000 nodes) than the studied PT-191 bus network, and can provide an optimal solution in a time which is reasonable to DSOs in day-ahead operation framework.

G. Comparison With the Method in [29] for S-MP-OPF

Table X shows the performance of linear power flow expressions [29] based S-MP-OPF model for PT-191 ADS operating under stressed condition.

In terms of optimality gap, one observes that [29] leads to a slightly higher optimality gap (although still less than 0.1% in all FOs) than the proposed SLA (see Table VIII).

In terms of solution feasibility, [29] provides an AC infeasible solution in FOs 4† and 4‡ as maximum constraint violation value becomes significantly higher than the thermal loading limit. The proposed SLA, on the other hand, provides AC feasible solution for these FOs.

In terms of computational time, [29] is slower for all FOs, except FO7, than the proposed SLA as it requires more outer-loop iterations to reach an optimal (and feasible) solution.

To conclude, the linear power flow expressions in [29] compare less favorably to the proposed SLA. This is mainly due to the small angle and near/flat voltage profile assumptions used in deriving the linear expressions, as stated previously, which ultimately capture less non-linearity, whereas the proposed linear expressions in this work are based on the second-order Taylor series expansion of trigonometric terms and novel linearization technique for $V_i V_j$ term. Resultantly, the proposed SLA outperforms [29], in terms of performance, as it captures better the non-linearity.

H. Evaluating the Optimality of Proposed SLA Solution

This section evaluates empirically the global optimality of SLA solution by comparing it with the results of mixed-integer second order cone programming (MISOCP)-based S-MP-OPF model [43], solved by CPLEX, as MISOCP provides the global optimal solution of original model M0 if the relaxation holds[2].

[2]In [43], the constraint $c_{ij}^2 + s_{ij}^2 = c_{ii} * c_{jj}$ is relaxed as $c_{ij}^2 + s_{ij}^2 \leq c_{ii} * c_{jj}$ and relaxation error is defined as $|c_{ij}^2 + s_{ij}^2 - c_{ii} * c_{jj}|$.

TABLE XI
GLOBAL OPTIMALITY OF PROPOSED SLA SOLUTION UNDER ACTIVE POWER LOSSES OBJECTIVE FUNCTION

FOs	Test Cases	Objective Value (pu)			Max. Relax. Error (pu)	Constraints Violation (MISOCP)		
		M0	MISOCP	SLA		No.	Max (%)	$\leq$1%
FO1	34-bus	18.1	17.2	18.1	8.50×10^{-3}	6820	4.7	826
	UK 31-bus	-0.280	-0.283	-0.282	2.40×10^{-6}	0	0	0
	PT 191-bus	0.647	0.645	0.647	3.50×10^{-7}	0	0	0

TABLE XII
PERFORMANCE OF MISOCP UNDER FLEXIBILITY PROCUREMENT OBJECTIVE FUNCTION

Test Cases	FOs	Optimality Gap (%)	Constraints Violations				Max. Relax. Error (pu)	Time (s)	
			No.	Max (%)	Avg (%)	$\leq$1%		M0	MISOCP
34 bus	FO4†	100.0	2799	10.9	1.1	1952	2.9×10^{-4}	16	15
	FO9†	100.0	2759	10.8	1.1	1964	3.5×10^{-4}	23	15
UK 31-bus	FO4†	33.1	7440	43.9	38.1	0	3.5×10^{-3}	3600	355
	FO9†	37.1	7440	65.9	39.1	0	4.8×10^{-3}	3600	2671
PT 191-bus	FO4†	85.1	45840	73.2	33.5	0	1.5×10^{-3}	3600	5597
	FO9†	70.9	45840	72.0	33.5	0	1.4×10^{-3}	3600	13508

$\dagger$: taps = 09.

Furthermore, the superiority of proposed SLA, in terms of provision of AC feasible solution, over MISOCP when relaxation fails to hold is also shown.

To assess the global optimality of obtained solution, M0, MISOCP and SLA methodologies are compared, as shown in Table XI, under active power losses objective function in all test cases for FO1. It can be seen that in the case of U.K. and PT ADSs, the MISOCP approach provides the global optimal solution as relaxation holds (maximum relaxation error is lower than 10^{-6}) in these test systems. Both M0 and SLA also converge to the same optimal solution, as MISOCP does, in these test cases. This indicates that model M0 and proposed SLA indeed provide the global optimal solution. Moreover, all three methodologies provide an AC feasible solution for the studied cases as shown in Table XI for MISOCP and Tables IV, VI and VIII for SLA.

On the other hand, in the case of flexibility procurement objective (1) for all test cases (Table XII) and active power losses minimization objective for 34-bus ADS (Table XI), the relaxation fails to hold as can be noticed by a large value of maximum relaxation error and AC infeasible solution (unrealistic voltage values, which severely violate voltage bounds, are obtained at the solution of MISOCP approach). This shows that MISOCP provides a lower bound to the objective value and the recovered solution is AC infeasible. On the other hand, both M0 and SLA converge to the same optimal value, as shown in Tables IV, VI and VIII for these FOs, and provide an AC feasible solution.

The presented results in Tables XI and XII bring further empirical evidence that proposed SLA not only provides a global optimal solution but is also capable of providing an AC feasible solution under different objective functions and FOs where MISOCP approach fails to provide a meaningful solution, hence its lower bound (optimality gap) is irrelevant.

Finally, in terms of computational time, MISOCP takes a large amount of time (1.5–3.5 hours) under increasing number of binary variables and quadratic constraints as can be seen in the case of FOs 4† and 9† for PT 191-bus ADS. This is partly because solvers for convex quadratic problems are still less mature as compared to the solvers for linear problems.

I. Concluding Remarks About the Accuracy, Scalability, Global Optimality and Stopping Criterion of the Proposed SLA

This section concludes the results, obtained for the three test systems, by summarizing the main findings about the performance of the proposed SLA.

In terms of solution accuracy, the proposed SLA is capable of providing practically the same optimal and feasible solution as obtained by the benchmark model M0 under normal and stressed operating conditions as shown for all test cases. The exception to this are few overload instances which violate the feasibility threshold under stressed operating conditions (FO7 in the PT test case). However, it must be kept in mind that reduction in thermal limit by 20% is a very tough case (given that the congestion already appears in the base case) and even under such scenario, the overload remains within 1.15%. Therefore, it can be safely concluded that the proposed linear approximations are robust and provide a highly accurate solution under both normal and strict operating conditions.

Regarding computational performance, SLA outperforms the benchmark model M0 in all test cases. The MINLP solver hits the maximum time limit in majority of FOs in all networks and, therefore, only provides the utopian lower bound on the optimal value. In comparison, the proposed SLA reduces the solution time by a factor of 13-30 in small size ADSs, whereas in large size ADS, the solution time is reduced by a factor of 12-18 under normal and stressed operating condition.

The solution time of proposed SLA strongly depends on the number of inner- and outer-loop iterations (i.e., the number of times a MILP problem is solved). A strict *trustable approximation* and *feasibility violation tolerance* criteria (as chosen in this paper) lead to more inner- and outer-loop iterations which, in turn, increase the overall solution time. Consequently, by considering tighter values of these criteria to improve the solution accuracy, the number of inner- and outer-loop iterations will increase which would, ultimately, lead to longer solution time.

The proposed SLA can be scalable to ADSs of around 1000 nodes by extrapolating the scalability test results and can provide an optimal solution within one-three hours, which is acceptable in day-ahead operation planning framework.

Regarding the quality of obtained solution from proposed SLA, empirical evidence shows that presented approach provides the global optimal solution as it leads to the same optimum as convex MISOCP does wherever relaxation holds. In cases where relaxation does not hold, the obtained solution from SLA has good chances to be the global optimum since extensive empirical evidence, presented in [44] and this paper, also points out that the solution provided by a local optimizer (e.g., IPOPT) is global optimum in most generic AC OPF problem instances. On the basis of this, it can cautiously concluded that the probability of obtaining the global optimum from model M0 is high and as such, the close vicinity of proposed SLA solution to the M0 solution also makes it the global optimal solution.

Finally, the stopping criteria of SLA i.e., the feasibility threshold targets primarily achieving an AC feasible solution of high quality (i.e., as close as possible to the global optimal). This paper adopts an industrial application mindset, which demands to shift the focus from mathematically rigorous optimization of ideal models to efficient improvements of imperfectly known real-world models [45]. On the basis of this, the presented algorithm, being an approximation, might not systematically achieve the same feasibility threshold as AC OPF (around 10^{-4} pu); however, for practical operation of power systems, such an accuracy is not really necessary given there exists other sources of uncertainty such as imperfect models, variability, noise, etc. As such, the chosen feasibility threshold of 1% (i.e., the value of nodes voltages and/or branch current *above 1% of their rated pu values* is deemed as an infeasible solution) is a good compromise between solution accuracy and time. Note that the obtained results achieve an even 10–100 times higher accuracy than the feasibility threshold (e.g., below 0.1%); as such, the good approximation of optimal solution is obtained as feasibility is reached.

J. Impact of Successive Linearization on Solution Accuracy

Table XIII shows the impact of performing successive linearization on the solution accuracy (optimality gap and AC feasibility) in all test cases, under representative stressed operating conditions, for FOs $4^{\dagger}$ and $9^{\dagger}$. Similar results are obtained for the other FOs, hence they are not shown. The following observations can be made from the provided results.

Single-step linearization (iteration 1) fails to achieve highly accurate results as evident by a large optimality gap and/or AC infeasible solution. In the case of 34-bus test system, large optimality gap is observed in both FOs albeit the obtained solution is AC feasible. On the other hand, for U.K. and PT test cases, an AC infeasible solution (branch current constraints are violated in all FOs and maximum violation values vary between 5%–10% above the rated value) is obtained. These results clearly show that single-shot linearization are prone to failure under stressed operating conditions or when operating conditions move significantly away from the PoL.

The proposed SLA corrects the linearization error and improves the solution accuracy in successive iterations as can be noticed in all test cases. Thanks to the chosen tight value of trustable approximation criterion, the SLA performs another iteration for 34-bus system (due to the non-satisfaction of this criterion in the first iteration) and brings the optimality gap below 0.30% while still staying in the feasible region. On the other hand, in the case of U.K. (FO4†) and PT (FO9†) systems, an AC feasible solution is obtained in the second iteration as well as the optimality gap is almost closed. However, SLA performs another iteration as the trustable approximation criterion is not satisfied. As such, the price of choosing a conservative value of this criterion is payed at the expense of an additional iteration; thus, more computation time. Lastly, for U.K. (FO9†) and PT (FO4†) cases, SLA gradually decreases the optimality gap and constraints violations in successive iterations until AC feasible solution of high accuracy is achieved.

To summarize, the proposed SLA is highly accurate and able to achieve the same results as the original model (M0) due to

TABLE XIII
IMPACT OF SUCCESSIVE LINEARIZATION ON SOLUTION ACCURACY

Test Cases	FOs	Optimality Gap (%) in Iterations						Initial Violation (%)		Constraints Violation (%) in Iterations											
										1		2		3		4		5		6	
		1	2	3	4	5	6	No.	Max	No.	Max	No.	Max	No.	Max	No.	Max	No.	Max	No.	Max
34-bus	FO4†	8.90	**0.06**	-	-	-	-	535*	12.4	0	0.0003	0	**0.0002**	-	-	-	-	-	-	-	-
	FO9†	13.1	**0.26**	-	-	-	-	535*	12.4	0	0.0003	0	**0.0002**	-	-	-	-	-	-	-	-
UK 30-bus	FO4†	0.19	0.002	**0.00**	-	-	-	24°	44.9	10	5.7	11	0.47	9	**0.22**	-	-	-	-	-	-
	FO9†	0.16	0.04	**0.05**	-	-	-	24°	44.9	12	10.1	13	1.61	2	**0.01**	-	-	-	-	-	-
PT 191-bus	FO4†	0.38	0.02	0.013	0.05	0.02	**0.011**	27°	36.2	21	7.2	18	1.23	14	1.01	3	3.31	13	1.49	3	**0.37**
	FO9†	0.49	0.05	**0.04**	-	-	-	27°	36.2	19	9.11	15	0.43	11	**0.03**	-	-	-	-	-	-

†: taps = 09; *: voltage violations; °: branch current violation;
bold font (**x**) indicates the termination of simulation after recovering an AC feasible solution.

TABLE XIV
PERFORMANCE OF SLA UNDER FLAT-START PoL

Test Cases	FOs	Optimality Gap (%)	Constraints Violations				Iter. IL/OL	Time (s)	
			No.	Max (%)	Avg (%)	≤1%		SLA°	SLA*
34-bus	FO4†	0.07	0	0.0002	0.0001	0	2/1	16	16
	FO9†	0.31	0	0.0002	0.0001	0	2/1	24	24
UK 30-bus	FO4†	0.33	5	0.93	0.33	5	3/2	20	110
	FO9†	0.24	4	0.97	0.25	4	3/3	28	127
PT 191-bus	FO4†	0.05	7	0.79	0.26	7	3/2	254	276
	FO9†	0.08	6	0.96	0.648	6	3/1	234	279

†: taps = 09; IL = inner loop; OL = outer loop.
°: SLA with initial PoL from AC PF; *: SLA with flat-start PoL.

the utilization and sequential enhancement of highly accurate proposed approximations.

K. Impact of Point of Linearization on Solution Accuracy

Table XIV presents the performance of proposed methodology using flat start as PoL in all test cases for FOs 4† and 9† under representative stressed operating conditions. Similar observations are noted for the remaining FOs. The presented results in Table XIV should be compared with the ones presented in Tables IV, VI and VIII to evaluate the impact of PoL on solution accuracy and computational efficiency of the proposed SLA. Distinct observations are as follows.

In terms of optimality gap, a slightly larger gap is obtained under flat start PoL in all test cases. Regarding AC feasibility of the recovered solution, both flat start and AC PF PoL based model M1 provides the similar results for 34-bus test system. However, in the case of U.K. and PT test cases, the maximum and average values of constraint violations are significantly higher (close to the feasibility threshold) when flat start PoL based model M1 is used. This suggests that an AC infeasible solution can be obtained when a system, being operated under stressed operating conditions, is modeled by less realistic assumptions such as flat start.

In terms of CPU time, the solution time increases significantly (almost 5 times), due to an increase in the number of SLA iterations, for the U.K. ADS, but only slightly (almost 1.2 times) for the PT ADS.

To conclude, these results indicate that flat start PoL based proposed model is more susceptible to less accurate results (large optimality gap and constraint violation magnitude) and higher solution time, particularly when operating conditions are far from ideal i.e., normal operating conditions.

VII. CONCLUSION

The paper presents a novel tractable sophisticated heuristic sequential linearization algorithm (SLA) for the S-MP AC-OPF model, aimed at flexibility procurement in day-ahead operation planning framework of ADSs. The proposed SLA is based on linear approximations of AC power flows and branch current expressions and subsequently their incorporation in a MILP model that is solved sequentially to enhance the approximation accuracy.

In terms of solution accuracy, the extensive results clearly demonstrate empirically that the proposed SLA provides an optimal and feasible solution. The optimality gap is nearly 0% (its worst value is 0.21%) in all test cases under all flexible options FOs 1-9. Similarly, in terms of constraints satisfaction, AC-feasible solution is obtained within few SLA iterations as well as the accuracy of developed linear approximations remains intact under tougher operation conditions.

Regarding computational efficiency, the proposed SLA reduces the solution time by a factor of 13-30 and 12-18 in small-size and large-size ADSs respectively, as compared to the benchmark model M0 when the latter converges. Also, the SLA outperforms clearly an alternative linear model [29]. Furthermore, the solution time of presented SLA remains moderate (below one hour) for the 191-bus ADS, thus hinting towards its practical application for real-world ADSs. To foster replicability and comparison, the open code source of the tool as well as the test cases from this work will be made available at https://zenodo.org/communities/attest-eu/?page=1&size=20

Finally, the proposed tractable approach can easily be applied to other S-MP-OPF problems containing binary and/or integer variables, such as optimal volt/var control in ADS etc.

REFERENCES

[1] A. Keane et al., "State-of-the-art techniques and challenges ahead for distributed generation planning and optimization," *IEEE Trans. Power Syst.*, vol. 28, no. 2, pp. 1493–1502, May 2013.

[2] M. Usman, M. Coppo, F. Bignucolo, and R. Turri, "Losses management strategies in active distribution networks: A review," *Electric Power Syst. Res.*, vol. 163, pp. 116–132, 2018.

[3] F. U. Nazir, B. C. Pal, and R. A. Jabr, "A two-stage chance constrained Volt/Var control scheme for active distribution networks with nodal power uncertainties," *IEEE Trans. Pwr. Syst.*, vol. 34, no. 1, pp. 314–325, Jan. 2019.

[4] T. Ding, C. Li, Y. Yang, J. Jiang, Z. Bie, and F. Blaabjerg, "A two-stage robust optimization for centralized-optimal dispatch of photovoltaic inverters in active distribution networks," *IEEE Trans. Sustain. Energy*, vol. 8, no. 2, pp. 744–754, Apr. 2017.

[5] T. Ding, S. Liu, W. Yuan, Z. Bie, and B. Zeng, "A two-stage robust reactive power optimization considering uncertain wind power integration in active distribution networks," *IEEE Trans. Sustain. Energy*, vol. 7, no. 1, pp. 301–311, Jan. 2016.

[6] M. Bazrafshan and N. Gatsis, "Decentralized stochastic optimal power flow in radial networks with distributed generation," *IEEE Trans. Smart Grid*, vol. 8, no. 2, pp. 787–801, Mar. 2017.

[7] Q. Gemine, E. Karangelos, D. Ernst, and B. Cornélusse, "Active network management: Planning under uncertainty for exploiting load modulation," in *Proc. IREP Symp. Bulk Power System Dyn. Control - IX Optim., Secur. Control Emerg. Power Grid*, 2013, pp. 1–9.

[8] G. Zou, Y. Ma, J. Yang, and M. Hou, "Multi-time scale optimal dispatch in ADN based on MILP," *Int. J. Elect. Power Energy Syst.*, vol. 102, pp. 393–400, 2018.

[9] S. Gill, I. Kockar, and G. W. Ault, "Dynamic optimal power flow for active distribution networks," *IEEE Trans. Pwr. Syst.*, vol. 29, no. 1, pp. 121–131, Jan. 2014.

[10] A. Gabash and P. Li, "Active-reactive optimal power flow in distribution networks with embedded generation and battery storage," *IEEE Trans. Pwr. Syst.*, vol. 27, no. 4, pp. 2026–2035, Nov. 2012.

[11] V. A. Evangelopoulos, I. I. Avramidis, and P. S. Georgilakis, "Flexibility services management under uncertainties for power distribution systems: Stochastic scheduling and predictive real-time dispatch," *IEEE Access*, vol. 8, pp. 38855–38871, 2020.

[12] T. Soares, R. J. Bessa, P. Pinson, and H. Morais, "Active distribution grid management based on robust AC optimal power flow," *IEEE Trans. Smart Grid*, vol. 9, no. 6, pp. 6229–6241, Nov. 2018.

[13] A. Eajal, M. F. Shaaban, K. Ponnambalam, and E. El-Saadany, "Stochastic centralized dispatch scheme for AC/DC hybrid smart distribution systems," *IEEE Trans. Sustain. Energy*, vol. 7, no. 3, pp. 1046–1059, Jul. 2016.

[14] H. Gao, J. Liu, and L. Wang, "Robust coordinated optimization of active and reactive power in active distribution systems," *IEEE Trans. Smart Grid*, vol. 9, no. 5, pp. 4436–4447, Sep. 2018.

[15] X. Yang, C. Xu, H. He, W. Yao, J. Wen, and Y. Zhang, "Flexibility provisions in active distribution networks with uncertainties," *IEEE Trans. Sustain. Energy*, vol. 12, no. 1, pp. 553–567, Jan. 2021.

[16] E. Dall'Anese, K. Baker, and T. Summers, "Chance-constrained AC optimal power flow for distribution systems with renewables," *IEEE Trans. Power Syst.*, vol. 32, no. 5, pp. 3427–3438, Sep. 2017.

[17] A. Baharvandi et al., "Linearized hybrid stochastic/robust scheduling of active distribution networks encompassing PVs," *IEEE Trans. Smart Grid*, vol. 11, no. 1, pp. 357–367, Jan. 2020.

[18] A. N. Toutounchi, S. Seyedshenava, J. Contreras, and A. Akbarimajd, "A stochastic bilevel model to manage active distribution networks with multi-microgrids," *IEEE Syst. J.*, vol. 13, no. 4, pp. 4190–4199, Dec. 2019.

[19] J. Soares, M. A. F. Ghazvini, N. Borges, and Z. Vale, "A stochastic model for energy resources management considering demand response in smart grids," *Electric Power Syst. Res.*, vol. 143, pp. 599–610, 2017.

[20] J. G. Robertson, G. P. Harrison, and A. R. Wallace, "OPF techniques for real-time active management of distribution networks," *IEEE Trans. Power Syst.*, vol. 32, no. 5, pp. 3529–3537, Sep. 2016.

[21] L. Gan and S. H. Low, "An online gradient algorithm for optimal power flow on radial networks," *IEEE J. Sel. Areas Commun.*, vol. 34, no. 3, pp. 625–638, Mar. 2016.

[22] E. Dall'Anese and A. Simonetto, "Optimal power flow pursuit," *IEEE Trans. Smart Grid*, vol. 9, no. 2, pp. 942–952, Mar. 2018.

[23] S. Bolognani and S. Zampieri, "On the existence and linear approximation of the power flow solution in power distribution networks," *IEEE Trans. Power Syst.*, vol. 31, no. 1, pp. 163–172, Jan. 2016.

[24] M. Chatzos, T. W. Mak, and P. Vanhentenryck, "Spatial network decomposition for fast and scalable AC-OPF learning," *IEEE Trans. Power Syst.*, vol. 37, no. 4, pp. 2601–2612, Jul. 2022.

[25] A. S. Zamzam and K. Baker, "Learning optimal solutions for extremely fast ac optimal power flow," in *Proc. IEEE Int. Conf. Commun., Control, Comput. Technol. Smart Grids*, 2020, pp. 1–6.

[26] L. Duchesne, E. Karangelos, and L. Wehenkel, "Recent developments in machine learning for energy systems reliability management," *Proc. IEEE Proc. IRE*, vol. 108, no. 9, pp. 1656–1676, Sep. 2020.

[27] F. Fioretto, T. W. Mak, and P. Van Hentenryck, "Predicting AC optimal power flows: Combining deep learning and lagrangian dual methods," in *Proc. AAAI Conf. Artif. Intell.*, 2020, vol. 34, pp. 630–637.

[28] S. H. Low, "Convex relaxation of optimal power flow–part II: Exactness," *IEEE Trans. Control Netw. Syst.*, vol. 1, no. 2, pp. 177–189, Jun. 2014.

[29] Z. Yang, H. Zhong, A. Bose, T. Zheng, Q. Xia, and C. Kang, "A linearized OPF model with reactive power and voltage magnitude: A pathway to improve the MW-only DC OPF," *IEEE Trans. Power Syst.*, vol. 33, no. 2, pp. 1734–1745, Mar. 2017.

[30] J. Yang, N. Zhang, C. Kang, and Q. Xia, "A state-independent linear power flow model with accurate estimation of voltage magnitude," *IEEE Trans. Pwr. Syst.*, vol. 32, no. 5, pp. 3607–3617, Sep. 2016.

[31] S. M. Fatemi, S. Abedi, G. Gharehpetian, S. H. Hosseinian, and M. Abedi, "Introducing a novel DC power flow method with reactive power considerations," *IEEE Trans. Power Syst.*, vol. 30, no. 6, pp. 3012–3023, Nov. 2015.

[32] T. Akbari and M. T. Bina, "Linear approximated formulation of AC optimal power flow using binary discretisation," *IET GTD*, vol. 10, no. 5, pp. 1117–1123, 2016.

[33] M. Usman and F. Capitanescu, "A new second-order linear approximation to AC OPF managing flexibility provision in smart grids," in *Proc. IEEE SEST Conf.*, 2021, pp. 1–6.

[34] O. Alsac, J. Bright, M. Prais, and B. Stott, "Further developments in LP-based optimal power flow," *IEEE Trans. Power Syst.*, vol. 5, no. 3, pp. 697–711, Aug. 1990.

[35] S. Mhanna and P. Mancarella, "An exact sequential linear programming algorithm for the optimal power flow problem," *IEEE Trans. Pwr. Syst.*, vol. 37, no. 1, pp. 666–679, Jan. 2022.

[36] A. Castillo, P. Lipka, J.-P. Watson, S. S. Oren, and R. P. O'Neill, "A successive linear programming approach to solving the IV-ACOPF," *IEEE Trans. Power Syst.*, vol. 31, no. 4, pp. 2752–2763, Jul. 2016.

[37] M. Usman and F. Capitanescu, "A stochastic multi-period AC OPF for provision of flexibility services in smart grids," in *Proc. IEEE PowerTech Madrid*, 2021, pp. 1–6.

[38] W. Wei, "Tutorials on advanced optimization methods," 2020, *arXiv:2007.13545*.

[39] G. Box, "Box and Jenkins: Time series analysis, forecasting and control," in *A Very British Affair*. Berlin, Germany: Springer, 2013, pp. 161–215.

[40] W. R. Powell, "An analytical expression for the average output power of a wind machine," *Sol. Energy*, vol. 26, no. 1, pp. 77–80, 1981.

[41] Open data sets from ATTEST projects. [Online]. Available: https://zenodo.org/communities/attest-eu/?page=1&size=20

[42] I. Dunning, J. Huchette, and M. Lubin, "Jump: A modeling language for mathematical optimization," *SIAM Rev.*, vol. 59, no. 2, pp. 295–320, 2017.

[43] S. E. Kayacik and B. Kocuk, "An MISOCP-based solution approach to the reactive optimal power flow problem," *IEEE Trans. Pwr. Syst.*, vol. 36, no. 1, pp. 529–532, Jan. 2021.

[44] C. Coffrin, H. L. Hijazi, and P. Van Hentenryck, "The QC relaxation: A theoretical and computational study on optimal power flow," *IEEE Trans. Power Syst.*, vol. 31, no. 4, pp. 3008–3018, Jul. 2016.

[45] F. Capitanescu, "Suppressing ineffective control actions in optimal power flow problems," *IET Gener., Transmiss. Distrib.*, vol. 14, no. 13, pp. 2520–2527, 2020.

Muhammad Usman (Member, IEEE) received the Master of Science degree in power engineering from the Technical University of Munich, Munich, Germany, in 2016, and the Ph.D. degree in electrical energy engineering from the University of Padova, Padua, Italy, in 2020. His research interests mainly include the modeling and analysis of medium- and low-voltage active distribution systems through optimization techniques, particularly single- and multi-phase optimal power flow approach and losses allocation, and for smart grid management.

Florin Capitanescu (Member, IEEE) received the Electrical Power Engineering degree from the Politehnica University of Bucharest, Bucharest, Romania, in 1997, and the Ph.D. degree from the University of Liège, Liège, Belgium, in 2003. Since 2015, he has been a Senior Researcher with the Luxembourg Institute of Science and Technology, Esch-sur-Alzette, Luxembourg. His research interests mainly include the application of optimization methods to the operation of transmission and active distribution systems, particularly optimal power flow approaches, power systems security, voltage instability, and smart sustainable buildings.